Presented at the 1975
IEEE/IAS Annual Meeting
Sept.28-Oct.2, 1975.

MODELING AND DESIGN OF CONTROLLED CURRENT INDUCTION MOTOR DRIVE SYSTEMS

E.P. Cornell T.A. Lipo
Corporate Research & Development
General Electric Company
Schenectady, New York

Summary

A dynamic model for current controlled induction motor drives is developed, and a transfer function approach to the transient response investigation is formulated by means of d-q variables in the synchronously rotating reference frame. A sample control strategy is discussed, and transfer functions for various combinations of input and output variables are presented. It is shown that both dynamic and static instabilities exist for open-loop operation, but a well-damped closed-loop response is possible if slip frequency and current magnitude control are imposed.

A comparison between the analytical transfer function transient performance predictions, the transient response predicted by the hybrid computer simulation, and actual laboratory tests is made using frequency response techniques. Bode plots are used to correlate the results between laboratory and analytical techniques. Hybrid computer and laboratory results are presented to show typical steady state characteristics and waveforms.

Introduction

Under certain operating conditions a voltage/frequency controlled induction motor drive operating either as a motor or generator can exhibit self-sustained oscillations about a steady-state operating point[1]. These oscillations are actual instantaneous rotor speed changes accompanied by variations in output torque, motor current, and input power. This operating point instability is directly related to the machine, load and other system parameters and is not associated with the pulsating torques which normally accompany operation from inverter power sources. Related forms of instability are present in current/frequency controlled induction motor drives. An invesitgation into the cause, method of analysis, and means for eliminating this instability problem is the subject of this paper.

It is shown that open-loop operation is unstable for most operating conditions, and control loops must be added to realize feasible operating points. The presence of open loop instability makes design of the closed loop control by purely laboratory techniques a difficult task. This paper presents an analytical design technique for finding the transfer function between a specific input command and a controlled output variable based on small-signal linearization. The frequency response corresponding to the appropriate transfer function is compared to the actual frequency response measured on a laboratory breadboard and also on a hybrid computer simulation of the system. The results demonstrate that transfer function techniques can be reliably used to synthesize the necessary slip frequency/current and speed control strategies.

Induction Motor Model for Controlled Current Operation

A system block diagram for a controlled current induction motor drive fed from a three-phase source is shown as Fig. 1. In general, the system consists of an ac/dc controlled rectifier bridge, a dc link smoothing reactor, a current-controlled inverter (CCI) and three-phase induction machine. The current source inverter is typically the auto-sequential type described by Ward[2] although other types are possible.

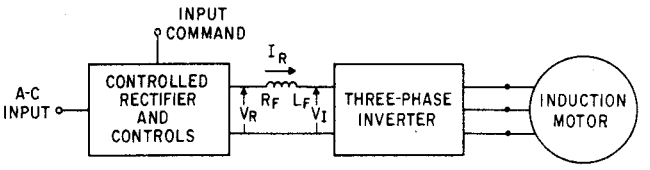

Fig. 1 Basic Controlled Current Inverter Induction Motor Drive System

When supplied from a current controlled inverter the motor phase currents are not sinusoidal but are rectangular in nature and flow for only 120 degrees of each half cycle (neglecting commutation effects). Ideally, only two phases conduct at any instant of time resulting in six distinct modes of operation[3]. A diagram illustrating the resulting line currents is shown in Fig. 2. If I_R is the magnitude of the current in the dc link, these stepped currents exciting the three stator phases can be represented by the Fourier series expansions given by Eqs. 1-3.

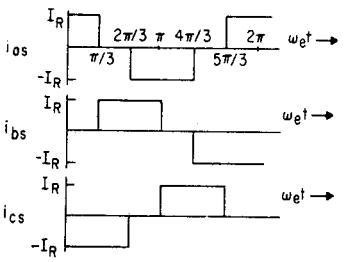

Fig. 2 Idealized Motor Line Currents

$$i_{as} = \frac{2\sqrt{3}}{\pi} I_R[\cos\omega_e t - \frac{1}{5}\cos 5\omega_e t + \frac{1}{7}\cos 7\omega_e t - \frac{1}{11}\cos 11\omega_e t + \ldots] \quad (1)$$

$$i_{bs} = \frac{2\sqrt{3}}{\pi} I_R[\cos(\omega_e t - 2\pi/3) - \frac{1}{5}\cos(5\omega_e t + 2\pi/3) + \frac{1}{7}\cos(7\omega_e t - 2\pi/3)\ldots] \quad (2)$$

$$i_{cs} = \frac{2\sqrt{3}}{\pi} I_R[\cos(\omega_e t + 2\pi/3) - \frac{1}{5}\cos(5\omega_e t - 2\pi/3) + \frac{1}{7}\cos(7\omega_e t + 2\pi/3)\ldots] \quad (3)$$

When performing stability or transfer function analyses, it is convenient to view the system in a reference frame that rotates around the airgap in synchronism with the stator MMF at a speed corresponding to stator excitation frequency. Machine voltage, flux and current variables become constant quantities during steady-state operation. These system equations represented in the synchronously rotating frame can thus be readily linearized around a particular steady-state operating point. Using the notation of Krause and Thomas[4], these induction machine equations are given in matrix form.

$$\begin{bmatrix} v_{qs}^e \\ v_{ds}^e \\ 0 \\ 0 \end{bmatrix} = \begin{bmatrix} r_s + \frac{p}{\omega_b}x_s & \frac{\omega_e}{\omega_b}x_s & \frac{p}{\omega_b}x_m & \frac{\omega_e}{\omega_b}x_m \\ -\frac{\omega_e}{\omega_b}x_s & r_s + \frac{p}{\omega_b}x_s & -\frac{\omega_e}{\omega_b}x_m & \frac{p}{\omega_b}x_m \\ \frac{p}{\omega_b}x_m & \frac{\omega_{s\ell}}{\omega_b}x_m & r'_r + \frac{p}{\omega_b}x'_r & \frac{\omega_{s\ell}}{\omega_b}x'_r \\ -\frac{\omega_{s\ell}}{\omega_b}x_m & \frac{p}{\omega_b}x_m & -\frac{\omega_{s\ell}}{\omega_b}x'_r & r'_r + \frac{p}{\omega_b}x'_r \end{bmatrix} \begin{bmatrix} i_{qs}^e \\ i_{ds}^e \\ i'^e_{qr} \\ i'^e_{dr} \end{bmatrix} \tag{4}$$

$$T_e = \frac{3}{2}\frac{p}{2}\frac{1}{\omega_b}x_m(i_{qs}^e\, i'^e_{dr} - i_{ds}^e\, i'^e_{qr}) = T_L + \frac{2J}{p}(p\omega_r)$$

In these equations, the superscript e is employed to denote that the d-q axes are synchronously rotating. A p denotes the operator d/dt. All reactance values are referred to base frequency such that the operator p/ω_b always appears. Although six equations are generally required to completely define the machine response, the two zero-sequence equations have been omitted since the sum of stator as well as rotor currents are zero. Also, in Eq. 4, ω_b is the base electrical angular velocity used to obtain the per unit machine parameters, ω_r is the equivalent electrical angular velocity of the rotor, and $\omega_{s\ell} = \omega_e - \omega_r$ is the slip angular frequency. The parameters r_s and r'_r are stator and referred rotor resistance referred to the stator. The quantities x_s, x_m and x'_r are the stator self-, mutual and rotor self-reactance referred to the stator respectively.

Using Eqs. 1-3 and applying the proper equations of transformation[4], the corresponding q- and d- axis currents in the synchronously rotating reference frame are

$$i_{qs}^e = \frac{2\sqrt{3}}{\pi}I_R\left(1 - \frac{2}{35}\cos 6\omega_e t - \frac{2}{143}\cos 12\omega_e t - \ldots\right) \tag{5}$$

$$i_{ds}^e = \frac{2\sqrt{3}}{\pi}I_R\left(-\frac{12}{35}\sin 6\omega_e t - \frac{24}{143}\sin 12\omega_e t - \ldots\right) \tag{6}$$

In Eqs. 5 and 6 the q- and the as- axes are assumed aligned at time t=0. For convenience, these currents can be expressed as

$$i_{qs}^e = I'_R\, g_{qs}^e \tag{7}$$

$$i_{ds}^e = I'_R\, g_{ds}^e \tag{8}$$

where g_{qs}^e and g_{ds}^e are the switching or "g" functions defined as

$$g_{qs}^e = 1 - \frac{2}{35}\cos 6\omega_e t - \frac{2}{143}\cos 12\omega_e t - \ldots \tag{9}$$

$$g_{ds}^e = -\frac{12}{35}\sin 6\omega_e t - \frac{24}{143}\sin 12\omega_e t - \ldots \tag{10}$$

and

$$I'_R = \frac{2\sqrt{3}}{\pi}I_R \tag{11}$$

It is important to note that Eqs. 7 and 8 are valid even if I_R is not constant.

Assuming no power loss in the inverter, the power into and out of the inverter is identical so that

$$V_I I_R = \frac{3}{2}(v_{qs}^e\, i_{qs}^e + v_{ds}^e\, i_{ds}^e) \tag{12}$$

The inverter voltage can be obtained by combining Eqs. 7, 8 and 12 as

$$V_I = \frac{3\sqrt{3}}{\pi}(v_{qs}^e\, g_{qs}^e + v_{ds}^e\, g_{ds}^e) \tag{13}$$

or simply

$$V'_I = v_{qs}^e\, g_{qs}^e + v_{ds}^e\, g_{ds}^e \tag{14}$$

where

$$V'_I = \frac{\pi}{3\sqrt{3}}V_I \tag{15}$$

Assuming continuous current in the smoothing reactor, the quantities I'_R and V'_I can be viewed as normalized dc link variables referred to the d-q axes. The differential equation expressing the dc link variables can be expressed in terms of normalized quantities as

$$V'_R = V'_I + (R'_F + \frac{p}{\omega_b}X'_F)I'_R \tag{16}$$

where it has been convenient to define new normalized link parameters

$$R'_F = \frac{\pi^2}{18}R_F \tag{17}$$

$$X'_F = \frac{\pi^2}{18}X_F \tag{18}$$

and also

$$V'_R = \frac{\pi}{3\sqrt{3}}V_R. \tag{19}$$

Eqs. 4, 7, 8, 14 and 16 form the basic system equations in the synchronously rotating reference frame and can be used to form the system equivalent circuit shown in Fig. 3. In Fig. 3, and subsequently in Fig. 4, it is assumed that the time derivative operator is (p/ω_b).

Although the actual system operates with rectangular-wave excitation from a high equivalent impedance source, it is well known that machine stability is determined primarily by the fundamental components of machine variables. If the effects of harmonics are ignored the "g" functions become simply

$$g_{qs}^{e} \cong 1.0 \tag{20}$$

$$g_{ds}^{e} \cong 0 \tag{21}$$

whereby, from Eqs. 7 and 8

$$i_{qs}^{e} = I_R' \tag{22}$$

$$i_{ds}^{e} = 0 \tag{23}$$

Because of the normalization employed, the current in the stator q-axis, I_R', corresponds to the peak value of the fundamental component of motor phase current. The d-axis stator current is identically zero during both steady-state and transient conditions due to the positioning of the synchronously rotating reference frame axes. From Eq. 14, orientation of the d-q axes also results in the identity that

$$v_{qs}^{e} = V_I' \tag{24}$$

with v_{ds}^{e} assuming the open-circuit value resulting from mutual coupling.

Neglecting harmonics, the detailed equivalent circuit of Fig. 3 reduces to the simplified equivalent circuit shown in Fig. 4.

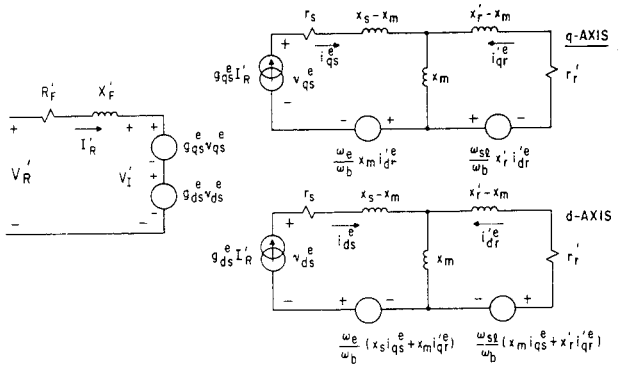

Fig. 3 d-q Equivalent Circuit of a CCI/ Induction Motor Drive in the Synchronously Rotating Reference Frame.

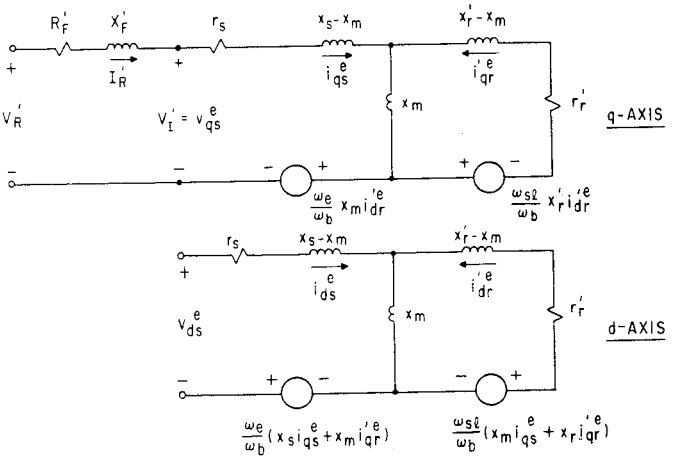

Fig. 4 Simplified d-q Equivalent Circuit

Equations 7 and 8 can be combined with the equations of the induction machine in the synchronously rotating reference frame to yield the corresponding system equations, Eqs. 25 and 26. Note that the ds equation in Eq. 25 has been omitted since i_{ds}^{e} is identically zero.

$$\begin{bmatrix} V_R' \\ 0 \\ 0 \end{bmatrix} = \begin{bmatrix} r_s + R_F' + \frac{p}{\omega_b}(x_s + X_F') & \frac{p}{\omega_b}x_m & \frac{\omega_e}{\omega_b}x_m \\ \frac{p}{\omega_b}x_m & r_r' + \frac{p}{\omega_b}x_r' & \frac{\omega_{s\ell}}{\omega_b}x_r' \\ -\frac{\omega_{s\ell}}{\omega_b}x_m & -\frac{\omega_{s\ell}}{\omega_b}x_r' & r_r' + \frac{p}{\omega_b}x_r' \end{bmatrix} \times \begin{bmatrix} i_{qs}^{e} \\ i_{qr}'^{e} \\ i_{dr}'^{e} \end{bmatrix} \tag{25}$$

$$T_e = \frac{3P}{4\omega_b}x_m\, i_{qs}^{e}\, i_{dr}'^{e} = T_L + \left(\frac{2J}{P}\right)p\omega_r \tag{26}$$

The steady-state slip-torque characteristics for a CCI/induction motor drive are shown in Fig. 5. The curves plotted in Fig. 5 were laboratory measured characteristics for an 18.5 kW machine. The parameters for the laboratory machine are given as Appendix I. These steady-state characteristics have been shown to correlate to within a few percent[3] of theoretical predictions using state-variable techniques.

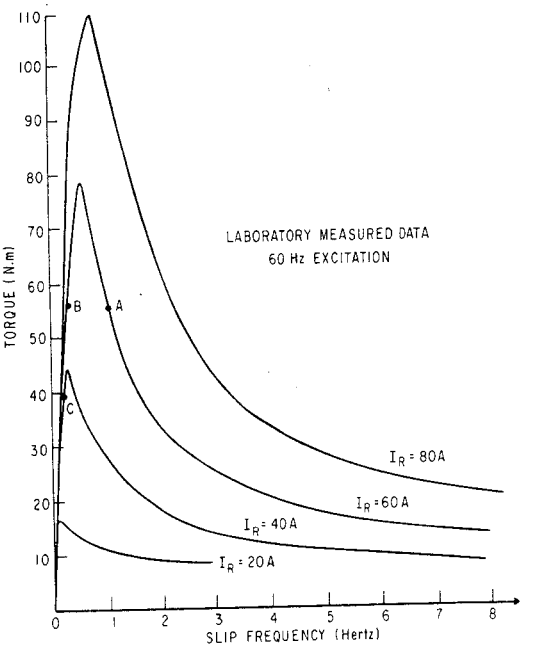

Fig. 5 Steady State CCI Motor Characteristics

Only a small portion of the slip-torque characteristics are shown. Examination of the characteristics indicate two regions of operation - one with a positive slope and the other with a negative slope.

The positive sloped portions are well known to be inherently unstable. This type of instability will be referred to as a static instability. It is also possible to have a dynamic instability on either portion of the characteristics. This is caused by negative electrical damping which is highly dependent on the selection of operating point and machine parameters. For CCI operation, the steady-state operating point can occur on either the upper or lower portion of the characteristic. For example, if operation is constrained such that the machine is never driven into a highly saturated condition, operation would be at Point A for T_e = 57 N.m. Operation at Point B, which yields the same output torque, corresponds to a highly saturated condition. For low torque and rated flux conditions, the steady-state operating point would be on the upper portion of a low current magnitude characteristic, for example, at Point C. Point C is on the statically stable side of the I_R = 40A characteristic. It is apparent that closed loop control is necessary to insure stable operation over the entire load range of CCI drives.

Calculation of CCI Transfer Functions

One method available to study the transient performance of electric drives is small signal linearization. Each variable is considered to be composed of a steady-state and small-time varying component. These components are substituted into the original non-linear equations. All purely steady-state terms drop out and all second order perturbations are ignored. The remaining equations are linear in the perturbation variables which allows the system designer to use linear control analytical techniques to synthesize the needed control. The linearized equations in matrix form are

$$\begin{bmatrix} (X'_F + x_s) & x_m & 0 & 0 \\ x_m & x'_r & 0 & 0 \\ 0 & 0 & x'_r & 0 \\ 0 & 0 & 0 & -\frac{2J\omega_b^2}{P} \end{bmatrix} \frac{p}{\omega_b} \begin{bmatrix} \Delta i^e_{qs} \\ \Delta i'^e_{qr} \\ \Delta i'^e_{dr} \\ \frac{\Delta\omega_r}{\omega_b} \end{bmatrix} +$$

$$\begin{bmatrix} r_s + R'_F & 0 & \frac{\omega_e}{\omega_b}x_m & 0 \\ 0 & r'_r & \frac{\omega_{s\ell}}{\omega_b}x'_r & -x'_r i'^e_{dro} \\ \frac{\omega_{s\ell}}{\omega_b}x_m & -\frac{\omega_{s\ell}}{\omega_b}x'_r & r'_r & x_m i^e_{qso} + x'_r i'^e_{qro} \\ \frac{3P}{4\omega_b}x_m i'^e_{dro} & 0 & \frac{3P}{4\omega_b}x_m i^e_{qso} & 0 \end{bmatrix} \begin{bmatrix} \Delta i^e_{qs} \\ \Delta i'^e_{qr} \\ \Delta i'^e_{dr} \\ \frac{\Delta\omega_r}{\omega_b} \end{bmatrix} =$$

$$\begin{bmatrix} -x_m i'^e_{dro} \\ -x'_r i'^e_{dro} \\ x_m i^e_{qso} + x'_r i'^e_{qro} \\ 0 \end{bmatrix} \frac{\Delta\omega_e}{\omega_b} + \begin{bmatrix} 1 \\ 0 \\ 0 \\ 0 \end{bmatrix} \Delta V'_R + \begin{bmatrix} 0 \\ 0 \\ 0 \\ 1 \end{bmatrix} \Delta T_L \qquad (27)$$

If both sides of this matrix equation are premultiplied by the coefficient matrix of the derivative vector, the resulting equations can be arranged in state variable form

$$\frac{p}{\omega_b}\begin{bmatrix} \overline{\Delta i} \\ \frac{\Delta\omega_r}{\omega_b} \end{bmatrix} = \bar{A}\begin{bmatrix} \overline{\Delta i} \\ \frac{\Delta\omega_r}{\omega_b} \end{bmatrix} + \bar{b}\overline{\Delta u} \qquad (28)$$

$$\text{where } \overline{\Delta i} = \begin{bmatrix} \Delta i^e_{qs} \\ \Delta i'^e_{qr} \\ \Delta i'^e_{dr} \end{bmatrix};\ \bar{b} = \begin{bmatrix} b_1, b_2, b_3 \end{bmatrix};\ \overline{\Delta u} = \begin{bmatrix} \frac{\Delta\omega_e}{\omega_b} \\ \Delta V'_R \\ \Delta T_L \end{bmatrix} \qquad (29)$$

A digital computer algorithm was used to find the transfer function[5] between an element of $\overline{\Delta u}$ and a specified output Δy of the form

$$\Delta y = \bar{c}^t \begin{bmatrix} \overline{\Delta i} \\ \frac{\Delta\omega_r}{\omega_b} \end{bmatrix} + \bar{d}^t\overline{\Delta u} \qquad (30)$$

For a specific input two of the three elements of $\overline{\Delta u}$ are set equal to zero. The transfer function is returned in factored form with the associated dc gain. Stability and transient response is immediately apparent from the pole-zero locations.

If open loop operation is attempted by applying an uncontrolled rectifier voltage and by commanding a constant inverter switching frequency (no current magnitude or slip control), the drive will accelerate into a saturated condition or slow down to zero speed. This can be predicted by calculating the transfer function $\Delta I'_R/\Delta V'_R$ and examining the pole-zero locations. The transfer function for open-loop operation corresponding to Points A, B and C on Fig. 5 are given as Table I[6].

Point	T_e (N.m)	$f_{s\ell}$ (Hz)	I_R (A)	dc Gain	Zeros	Poles
A	57	1.2	60	-2.10	+8.25 -6.69±j15.7	+11.1±j14.7 -22.2±j24.1
B	57	.13	60	-1.48	-2.30 -1.41±j34.5	+41.3 -2.38 -30.5±j54.5
C	40	.34	40	-.42	-.76 -2.18±j17.8	+32.0 -.833 -26.6±j39.5

Table I - Open Loop Transfer Function $\Delta I'_R/\Delta V'_R$ for f_e = 60 Hz.

It can be noted that the system is dynamically unstable at all four operating points. This type of instability results in one right-half plane pole in the linearized transfer function. In addition, for unsaturated conditions with sizable torque output, the system is also statically unstable which results in a second pole in the right-half plane at Point A. These results are indicative of all operating points in both

the motoring and regenerating region. If open-loop operation is attempted, the system will either slow down to zero speed or speed up and operate in a very highly saturated condition. Closed-loop control is imperative for stable operation.

Closed Loop Control

Examination of Eq. 27 suggests that two control variables are available for system stabilization. These system inputs are the rectifier voltage and the frequency command to the inverter. An elementary closed loop control which results in stable operation for full motoring and regenerative operation is the independent current magnitude and slip frequency control shown in Fig. 6.

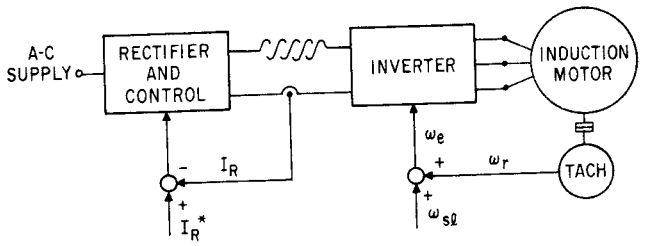

Fig. 6 Independent Current and Slip Frequency Control

With slip frequency control, incremental changes in rotor speed are related to incremental changes in electrical frequency by the constraint

$$\Delta\omega_e = \Delta\omega_r + \Delta\omega_{s\ell} \tag{31}$$

Slip frequency control forces electrical frequency to change in response to rotor speed, which tends to maintain a constant angular displacement between rotor and stator MMF's during both steady state and transient conditions. Although this type of control has a stabilizing effect, it is not capable of ensuring stable operation under all operating conditions. To obtain steady-state current control along with improved system transient response, the rectifier voltage must be constrained to respond to the error between a commanded value and the actual value of the dc link current. An integral plus proportional controller is used to give a satisfactory speed of response with zero steady-state error.

$$\frac{\Delta V'_R}{(\Delta I'^*_R - \Delta I'_R)} = \frac{K_c(1+\tau p)}{p} \tag{32}$$

To include the compensator in the analysis, a fifth state variable must be defined. ΔQ is defined to be the output of the integral controller, that is

$$\Delta Q = \frac{K_c}{p}(\Delta I'^*_R - \Delta I'_R) \tag{33}$$

The rectifier voltage can then be expressed as

$$\Delta V'_R = \Delta Q\,(1+\tau p) \tag{34}$$

The system matrix equation including the slip frequency and current magnitude control is

$$\begin{bmatrix} r_s + R'_F + \frac{p}{\omega_b}(x_s + X'_F) & \frac{p}{\omega_b}x_m & \frac{\omega_e}{\omega_b}x_m & -1-\tau p & x_m i'^e_{dro} \\ \frac{p}{\omega_b}x_m & r'_r + \frac{p}{\omega_b}x'_r & \frac{\omega_{s\ell}}{\omega_b}x'_r & 0 & 0 \\ -\frac{\omega_{s\ell}}{\omega_b}x_m & -\frac{\omega_{s\ell}}{\omega_b}x'_r & r'_r + \frac{p}{\omega_b}x'_r & 0 & 0 \\ K_c & 0 & 0 & p & 0 \\ \frac{3Px_m i'^e_{dro}}{4\omega_b} & 0 & \frac{3Px_m i^e_{qso}}{4\omega_b} & 0 & \frac{-2J\omega_b^2(\frac{p}{\omega_b})}{P} \end{bmatrix} \begin{bmatrix} \Delta i^e_{qs} \\ \Delta i'^e_{qr} \\ \Delta i'^e_{dr} \\ \Delta Q \\ \frac{\Delta\omega_r}{\omega_b} \end{bmatrix}$$

$$= \begin{bmatrix} -x_m i'^e_{dro} \\ -x'_r i'^e_{dro} \\ (x_m i^e_{qso} + x'_r i'^e_{qro}) \\ 0 \\ 0 \end{bmatrix} \frac{\Delta\omega_{s\ell}}{\omega_b} + \begin{bmatrix} 0 \\ 0 \\ 0 \\ K_c \\ 0 \end{bmatrix} \Delta I'^*_R + \begin{bmatrix} 0 \\ 0 \\ 0 \\ 0 \\ 1 \end{bmatrix} \Delta T_L \tag{35}$$

Since torque is proportional to the square of current, note that this type of control is essentially a torque control. In order to optimize performance, slip frequency must be adjusted with current to yield rated flux in the airgap. As can be seen by the pole zero locations in Table II, good transient characteristics occur at all operating points from full motoring to full regenerating. This type of response is indicative of operation at all rotor speeds within normal motor limitations.

T_e (N.m)	$f_{s\ell}$ (Hz)	I_R (A)	dc Gain	Zeros	Pole
101	1.20	82.	1.00	-8.03 -9.26 -2.55±j7.54	-3.71 -11.48 -4.01±j -229.
50	.45	45	1.00	-8.15 -9.17 -2.54±j2.85	-2.48 -11.04 -4.77±j3 -230.
0.1	.001	29	1.00	-2.54±j2.85 -8.10 -9.22	-2.45 -2.70 -7.97 -8.91 -231.
-50	-.45	45	1.00	-7.67 -.950 -2.61±j2.79	-6.52 -13.53 -1.54± -230.
-101	-1.20	82	1.00	-8.11 -9.19 -2.55±j7.54	-6.01 -15.5 -1.00 -229.

Table II - Transfer Function $\Delta I'_R/\Delta I'^*_R$ with independent slip frequency and current magnitude control for rated rotor speed operation with rated airgap flux.

Correlation with Test Results

In order to establish the validity of the transfer function approach two independent techniques were employed. The first technique utilized a hybrid computer system simulation in which the motor, the inverter, the rectifier, and the external feedback controls are all represented by simulating the appropriate algebraic and differential equations. The second technique involved frequency response measurements on actual laboratory hardware.

Fig. 7 shows a hybrid computer simulation recording of operation of an 18.5 kW CCI/induction motor drive used for laboratory evaluation. Included in this trace are motor current, i_{as}, line-neutral motor volts, v_{as}, inverter voltage, V_I, rectifier voltage, V_R, the actual current in the rotor of the machine, i_{ar}, the q- and d- axis stator currents in the synchronously rotating reference frame, i_{qs}^e, i_{ds}^e, and the developed electromechanical torque, T_e. It should be noted that these waveforms corroborate the predictions made using state variable techniques[3].

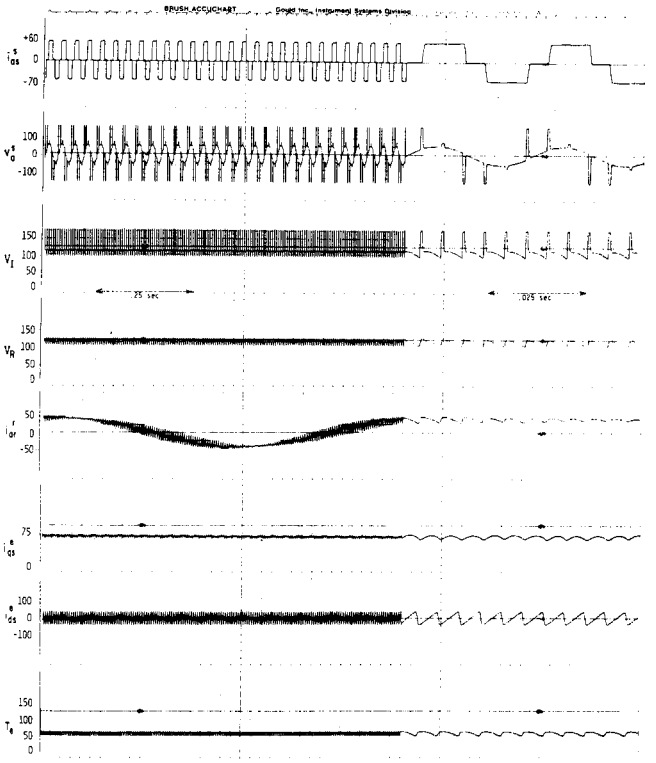

Fig. 7 Hybrid Computer Output of a CCI Drive Operating at Half-Speed and Half-Load.

Of special interest are the d- and q- axis stator current waveshapes in the synchronously rotating reference frame. These currents are directly proportional to the switching functions presented as Eqs. 9 and 10 with the proportionality constant, I_R. Neglecting all but the fundamental component in the transient response analyses results in $i_{ds}^e = 0$ and $i_{qs}^e = I_R$. Using the simulation, it was established that system transients do not introduce any substantial changes in these assumed constraints.

In order to verify transfer function predictions of actual transient response, frequency response measurements were made on the computer simulation using a low frequency range servo-analyzer. Since the simulation is time scaled down to 1/20 of real time, and maximum output voltage is ±10 volts, these tests must be run with extreme care to insure accuracy. It is well known that speed variations add a pole and zero that nearly cancel for normal values of inertia. Therefore, to reduce the complexity of the frequency response output, speed variations were removed from the analysis by assuming infinite system inertia. This modification also has the effect of removing any static instability that may be present if control synthesis is being attempted using hybrid computer techniques.

Steady state Point A on Fig. 5 was selected as the sample operating point for correlation of various techniques. The transfer function of actual dc link current over commanded link current with constant slip frequency and constant speed operation was computed as

$$\frac{\Delta I_R}{\Delta I_R^*} = \frac{1.0\,(s/1.99+1)\,(s^2/63.41 + s/12.35 + 1)}{(s/1.52+1)(s/333.+ 1)(s^2/80.0 + s/14.70 + 1)} \qquad (36)$$

The frequency response corresponding to this transfer function is plotted on Fig. 8 along with the frequency response measured directly from the hybrid computer simulation.

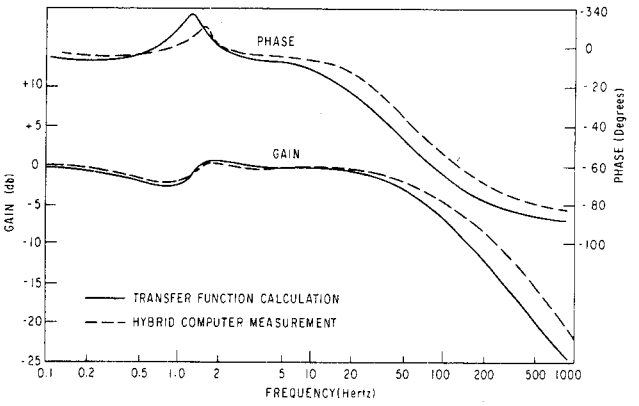

Fig. 8 Frequency Response Data for $\Delta I_R/\Delta I_R^*$ for I_R = 60A, $f_{s\ell}$ = 1.2 Hz, T_e = 51 N.m, n_r = 900 rpm.

Fig. 9 corresponds to similar operating conditions as used for Fig. 8, but represents the transfer function of actual dc link current over slip frequency.

$$\frac{\Delta I_R}{\Delta \omega_{s\ell}} = \frac{-2.9 \times 10^{-5}(s/4.95 \times 10^{-5} - 1)(s/18.67 - 1)}{(s/1.52+1)(s/333+1)(s^2/80.0 + s/14.70 + 1)} \qquad (37)$$

Note all transfer functions for the same operating condition have the same poles but different zeros. In both cases correlation between hybrid computer measured and digital computer prediction of the frequency response was found to be very good.

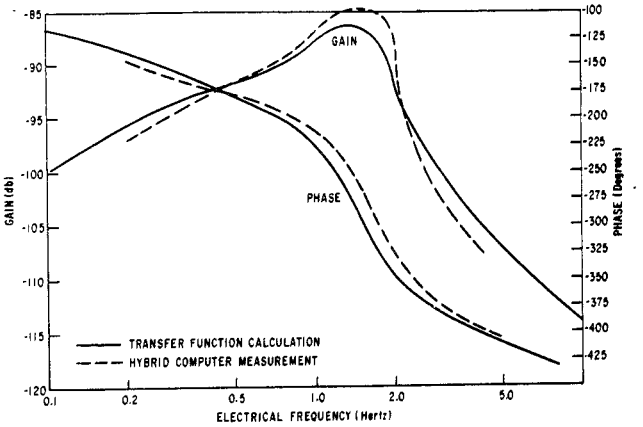

Fig. 9 Frequency Response Data for $\Delta I_R/\Delta\omega_{s\ell}$ for I_R = 60A, $f_{s\ell}$ = 1.2 Hz, T_e = 51 N.m.

As a second verification of the transfer function approach, actual laboratory frequency response measurements were conducted. The laboratory setup consists of an induction motor coupled to a dc load machine through a shaft torque transducer. The load machine is fed by an elementary Ward-Leonard system. In this case speed cannot be held constant, so that the load dynamics must be included in the analysis. This was done in the analysis by constraining changes in load torque, ΔT_L, to be proportional to changes in rotor speed, $\Delta\omega_r$.

The transfer function relating actual to commanded values of dc link current including speed variations is

$$\frac{\Delta I_R}{\Delta I_R^*} = \frac{1.0(s/8.04+1)(s/9.25+1)(s^2/54.30+s/10.61+1)}{(s/4.85+1)(s/10.95+1)(s/230+1)(s^2/73.65+s/10.55+1)} \quad (38)$$

This transfer function is correlated with laboratory measurements in Fig. 10.

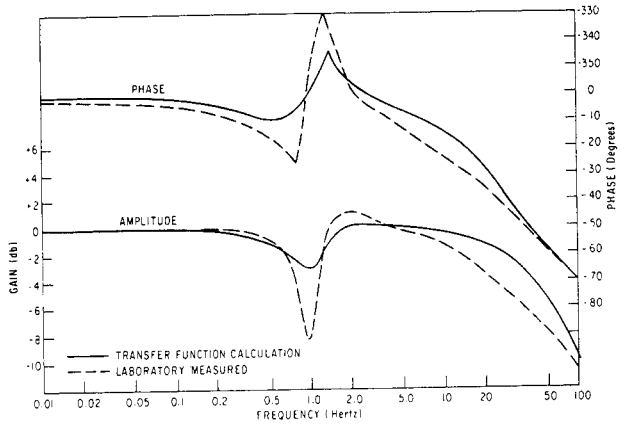

Fig. 10 Frequency Response for $\Delta I_R/\Delta I_R^*$ - I_R = 60A, $f_{s\ell}$ = 1.2 Hz, n_r = 875 rpm, T_e = 54 N.m.

The corresponding transfer function for changes in dc link current over changes in slip frequency is

$$\frac{\Delta I_R}{\Delta\omega_{s\ell}} = \frac{1.47\times10^{-4}(s/5.88\times10^{-4}-1)(s/15.4-1)(s/9.87+1)}{(s/4.85+1)(s/10.95+1)(s/230+1)(s^2/73.65+s/10.55+1)} \quad (39)$$

Fig. 11 compares predicted response to actual laboratory measurements. These measurements indicate that the actual system response is somewhat less damped than the transfer function predictions. A more accurate representation of the load dynamics would be needed for better correlation of results.

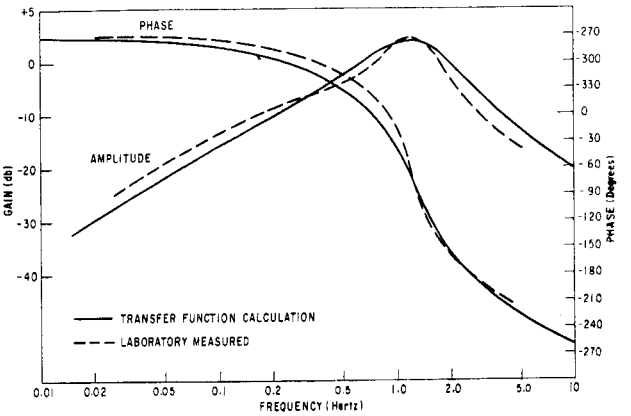

Fig. 11 Frequency Response for $\Delta I_R/\Delta\omega_{s\ell}$ - I_R = 60A, $f_{s\ell}$ = 1.2 Hz, n_r = 875 rpm, T_e = 54 N.m.

Other Closed Loop Controls

Transfer function techniques have also been used to synthesize more sophisticated controls for CCI operation. An interesting example has been reported in the literature[6], and a block diagram of the system is shown in Fig. 12.

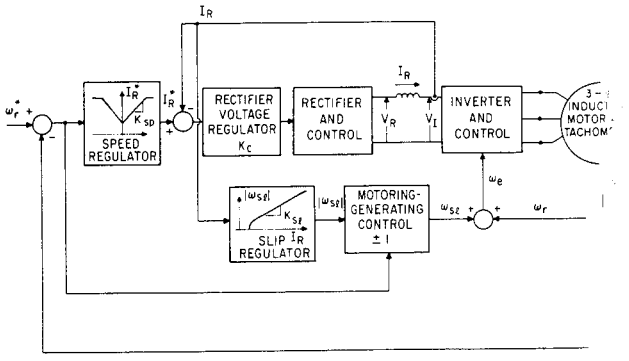

Fig. 12 Closed Loop CCI Speed Control

In this system slip frequency is forced to respond to changes in current magnitude in order to maintain constant flux in the airgap during both steady-state and transient conditions. That is

$$\Delta\omega_{s\ell} = K_{s\ell}\,\Delta I_R \qquad (40)$$

where $K_{s\ell}$ is chosen to maintain constant flux during a perturbation at a particular operating point. This constraint removes slip frequency as a system input. The two principle advantages of this constraint are that motor performance is optimized, and operation in the saturated rectifier voltage condition is possible (rectifier full on) because the slip frequency channel coupled to dc link current provides a stabilizing mechanism for the system. Speed control is obtained with a simple proportional controller.

$$\Delta I_R^* = K_{sp}\,(\Delta\omega_r^* - \Delta\omega_r) \qquad (41)$$

Conclusions

The feasibility of developing controlled current/induction motor drives using transfer function techniques has been established. A dynamic linearized model was used as the basis of the transient response study. Open loop operation was shown to correspond to an unstable operating condition. It was shown that independent current magnitude and slip frequency control is capable of stabilizing the drive system for all operating points in the motoring and regenerating modes of operation.

Frequency response measurements made on a hybrid computer simulation and actual laboratory hardware establish the validity of this approach. An improved CCI drive was presented which provides additional system damping by constraining slip frequency to respond to changes in dc link current.

References

(1) T.A. Lipo and P.C. Krause, "Stability analysis of a rectifier-inverter induction motor drive", IEEE Trans. on Power Apparatus and Systems, Vol. PAS-87, No. 1, January 1968, pp. 227-234.

(2) E.E. Ward, "Invertor suitable for operation over a range of frequency", Proceedings of IEE, Vol. III, No. 8, August 1964, pp. 1423-1434.

(3) T.A. Lipo and E.P. Cornell, "State variable steady-state analysis of a controlled current induction motor drive", IEEE Conference Record of the IAS 1974 Ninth Annual Meeting, October 7-10, 1974, Pittsburgh, Pa., Part II, pp. 851-859.

(4) P.C. Krause and C.H. Thomas, "Simulation of symmetrical induction machinery", IEEE Trans. on Power Apparatus and Systems, Vol. PAS-84, November 1965, pp. 1038-1053.

(5) T.A. Lipo and A.B. Plunkett, "A novel approach to induction motor transfer functions", IEEE Trans. on Power Apparatus and Systems, Vol. PAS-93, No. 5, September/October 1974, pp. 1410-1418.

(6) E.P. Cornell and T.A. Lipo, "Design of controlled current ac drive systems using transfer function techniques", Conference Record of IFAC Symposium on Control in Power Electronics and Electrical Drives, Duesseldorf, October 7-9, 1974, Vol. I, pp. 133-147.

Appendix I

Nameplate Motor Data	Motor & Filter Parameters
18.6 kW	$r_s = 0.0788\ \Omega$
4 Pole	$r_r' = 0.0408\ \Omega$
3 Phase, Y-connected	$x_s = 5.7518\ \Omega$
$\omega_b = 377$ rad/sec	$x_r' = 6.0028\ \Omega$
$J_{TOTAL} = 0.31$ Kg-m^2	$X_F = 5.50\ \Omega$
$V_{rated} = 230$V rms	$R_F = 0.091\ \Omega$
$I_{rated} = 64$A rms	

Nomenclature

In general:

Subscripts have the following meaning -

- o: steady state quantity as in i'^{e}_{dro}
- d or q: equivalent 2-phase transformed variable as in i^{e}_{ds}
- b: base quantity as in ω_b
- e: electrical quantity as in ω_e
- F: smoothing choke parameter as in R_F'
- I: inverter quantity as in V_I
- m: mutual value as in x_m
- ℓ: leakage quantity
- r: rotor quantity as in x_r
- R: rectifier quantity as in V_R
- s: stator quantity as in x_s
- $s\ell$: slip quantity as in $\omega_{s\ell}$

Superscript -

- *: command value as in ω_r^*
- ': rotor quantity referred to the stator or as noted in text
- e: quantities in synchronously rotating reference frame as i'^{e}_{dr}

Variables -

- Δ: perturbation variable
- τ: voltage regulator zero location
- ω: angular velocity
- V: dc voltage
- J: system inertia
- K_{sp}: speed regulator gain

$K_{s\ell}$: slip channel gain

K_c: compensator gain

p: differential operator d/dt

P: machine poles

Q: output of integral controller